Irrigation indices in almond:
a comparison with an improved sap flow method

By

HEATHER K. VICE

THESIS

Submitted in partial satisfaction of the requirements for the degree of

MASTER OF SCIENCE

in

Horticulture and Agronomy

in the

OFFICE OF GRADUATE STUDIES

of the

UNIVERSITY OF CALIFORNIA

DAVIS

Approved:

Thomas N. Buckley, Chair

Bruce D. Lampinen

Andrew J. McElrone

Committee in Charge

2021

ABSTRACT

Irrigation indices in almond: a comparison with an improved sap flow method

Heather K. Vice, Master of Science, 2021

Reliable strategies to assess crop water use are a persistent challenge across the agricultural sector with predicted shifts in annual precipitation patterns. Sap flow techniques provide valuable measurements of transpiration within a given plant, and thus may be useful for informing irrigation, but there are many methods from which to choose. It is also unclear how to best use sap flow data to effectively detect stress thresholds required to trigger irrigation events. The aim of the present work was to assess the potential to use continuous estimates of plant water use provided by sap flow as a complement to, or substitute for other plant-based irrigation predictors. I examined the suitability of three heat pulse methods — the double-ratio, heat-ratio and compensation heat-pulse methods (DRM, HRM and CHPM) — to estimate normalized sap velocity (NV) and normalized isothermal canopy conductance (NG, [$\propto$ NV/VPD]) in almond [*Prunus dulcis* (Miller) D.A. Webb] orchards located in a semi-arid Mediterranean environment. Measurements of sap flow in twelve 20-year-old trees and three irrigation demand indices — estimated crop evapotranspiration (ET_c), soil water content (θ) and stem water potential (Ψ_{stem}) — were conducted during two growing seasons, from June to September 2016 and 2017.

During well-watered periods of July, transpiration measures given by all irrigation indices demonstrated the limitations of Ψ_{stem} and θ as reliable indicators of plant water stress. Both sap flow and canopy conductance elicited clear patterns of the fluctuations in transpiration responses to changes in both θ and high evaporative demand in August, when irrigation was reduced for

harvest, declining in response to low θ in comparison to relatively high unchanging rates of ET_c. Ψ_{stem} followed a similar, yet slower, pattern illustrating the relationship between V_{DRM} and Ψ_{stem}, consistent with the concept of the "baseline" water potential varying with VPD. NG plateaued early in the day and decreased much earlier than V_{DRM} in the afternoon, indicating stomatal closure in response to elevated VPD. These data confirm the robust performance of the DRM in almond trees and reveal that stomatal regulation of transpiration in almond is more sensitive to VPD when θ is low. Normalized isothermal canopy conductance inferred from V_{DRM} and VPD is a promising and easily-implemented tool for interpreting short- and long-term dynamics of almond tree water status and their responses to abiotic stress.

KEYWORDS: Sap flow, Evapotranspiration, *Prunus dulcis,* Water deficit, Canopy conductance, Almonds, Irrigation tool, Evaporative demand, Soil water content, Plant water status, Stem water potential

DEDICATION

I dedicate this thesis to my daughter, Stella Rae Vice-Gatty, and my late grandmother, Lola V. Brothers, who inspire me daily to care for all things living.

ACKNOWLEDGEMENTS

I am most grateful to my advisor, Tom Buckley, for his expertise, full support and humor. Thanks to you, I stayed on this decade long journey.

This study was funded in part by The Almond Board of California through its Research and Innovation program. I am grateful to their staff as well for their assistance.

My sincere gratitude and appreciation to Matthew E. Gilbert for his dedicated mentorship, field and laboratory assistance. Also, my thank you to my committee members, Bruce Lampinen and Andrew McElrone for their time and very helpful advice.

My appreciation and deep thanks to all my fellow cohorts, friends, and family, especially my parents, without all of whom I could not have persevered.

TABLE OF CONTENTS

LIST OF TABLES AND FIGURES

MOST USED ABBREVIATIONS AND SYMBOLS

Symbol or Abbreviation	*Description*	*Units*
CHPM	Compensation Heat Pulse Method	--
DRM	Double Ratio Method	--
ET_{ref}	reference evapotranspiration	mm h^{-1} or day^{-1}
ET_c	crop evapotranspiration	mm h^{-1} or day^{-1}
HRM	Heat Ratio Method	--
γ	psychrometric constant	kPa $°C^{-1}$
H	soil heat flux density	MJ m^{-2} h^{-1}
K_c	crop coefficient	--
K	thermal conductivity	W m^{-1} K^{-1}
k	thermal diffusivity	cm^2 s^{-1}
θ	soil water content	m^3 m^{-3} or %
Ψ_{stem}	midday stem water potential	MPa
ρ_b	dry bulk density	g cm^{-3}
R_n	net shortwave solar radiation	MJ m^{-2} h^{-1}
R_s	global solar radiation	MJ m^{-2} h^{-1}
T	air temperature	^oC
t	time	sec
μ_2	wind speed	m s^{-1}
VPD	vapor pressure deficit	kPa
V_h	sap velocity	cm h^{-1}

1. INTRODUCTION

Projections of regional climate change include enhanced temperatures, severe droughts and unpredictable precipitation patterns for California throughout the remainder of the century. Two recent studies on climate change in California support previous findings that anthropogenic warming from greenhouse gas emissions has the potential to increase both variability in annual precipitation (Zhou *et al*. 2020) and the risk of long-term droughts (up to 35 years) by more than half, with an even higher (80%) likelihood for decade long droughts (Ullrich *et al*. 2018). The uncertainties and prevalence of both events can have substantial implications for water resource management across all agricultural sectors. To optimize agricultural water allocation, it may be necessary to adopt plant-based monitoring methods, which are sensitive to crop development, stress and production. Despite the numerous studies conducted on orchard system water use, an efficient, reliable. and scalable plant-based standard for high frequency irrigation scheduling of tree crops is lacking.

In California, where almonds [*Prunus dulcis* (Mill.) Webb] are the leading export crop, occupying 550,372 ha on 17% of California's irrigated cropland and producing $5.6 billion in annual revenue (CDFA 2018), recent resource management strategies outlined by the state require reductions in water consumption through agricultural water use efficiency (CDWR 2016). Thus, an understanding of the differences in water use by the commonly cultivated almond varieties for the development of innovative and accessible resource management tools is especially important. Several strategies are commonly used to assess irrigation needs in almond orchards. One method is to estimate crop evapotranspiration (ET_c) as the product of reference evapotranspiration (ET_{ref}), calculated from micrometeorology measurements obtained by remote sensing or nearby weather stations such as CIMIS (California Irrigation Management Information System), and an almond

crop coefficient multiplier (K_c; Doll 2020). Other methods include measurements of soil moisture content (volumetric [θ] or tension) (Andreu *et al.* 1997), as well as plant-based methods including diurnal trunk diameter fluctuation (Goldhamer and Fereres 2004; Egea *et al*. 2009) and stem water potential (Ψ_{stem}; Shackel 2010). Plant-based techniques can better capture spatiotemporal variations in plant water demand than traditional crop coefficients, yet their adoption has been slow, due to expense, both in terms of money and time. No current and widely used method offers continuous evaluation of plant-water status.

By contrast, sap flow – which is closely linked to transpiration and equivalent to it when integrated over a diel cycle (Espadafor *et al*. 2015) – can provide information not only about water demand, but also about water status: when combined with estimates of evaporative demand from micrometeorological data, sap flow can be used to calculate canopy conductance, which is closely linked to stomatal conductance, an important and water-stress-sensitive physiological parameter. Many sap flow techniques have been developed to study woody perennials. However, there is no current sap flow method that provides adequate resolution across high, low and reverse flows and is based on a single coherent measurement principle. The heat-ratio method (HRM; Marshall 1958; Burgess *et al*. 2001) cannot detect high flows, whereas the compensation heat-pulse method (CHPM; Swanson and Whitfield 1981, Green and Clothier 1988) cannot detect low or reverse flows (see Bleby *et al*. 2004, for an evaluation of the constraints of both methods). Alternative methods suffer from high power demands (e.g., Granier's constant power method; 1987) and limited usefulness on thicker tree trunks (e.g., the heat balance method; Shackel *et al*. 1992). There have been recent attempts to develop techniques without these shortcomings, but these are either poorly validated and computationally demanding (Vandegehuchte and Steppe 2012) or require switching between two different measurement principles at arbitrary intermediate flow rates

(Pearsall *et al*. 2014). Deng *et al*. (2021) recently proposed a novel technique, the double-ratio method (DRM), which overcomes these limitations. Conveniently, a DRM probe installation also provides the raw data needed to apply the HRM and CHPM techniques, enabling all three methods to be evaluated concurrently.

Almonds are grown in semi-arid Mediterranean environments where they are exposed to periods of wet-dry cycles along with periods of deficit irrigation imposed at harvest. Previous studies have investigated the effects of water stress in almonds, some focusing on periods of deficit irrigation (e.g., Goldhamer and Viveros 2000; Stewart *et al*. 2011) and others on genotype responses (e.g., Yadollahi *et al*. 2011). However, few experiments have explored the use of sap flow in almonds as a tool to detect water stress. A single method spanning low and high flows would be useful in almond, which has exceptionally high diurnal flows (Spinelli *et al*. 2017) combined with low nocturnal flows. The accuracy of existing sap flow methods in almond, and their capacity to quantify the drivers of transpiration, is poorly characterized. For example, one recent study found that the CHPM underestimated water uptake in almond by 31% (Phogat *et al*. 2012), while another study found CHPM to be consistent with lysimeter measurements of transpiration (Nortes *et al*. 2009). At the same time, researchers found that the CHPM had poor resolution for determining crop water consumption when used to monitor and schedule irrigation remotely in almonds and walnuts (Romero *et al*. 2008). To my knowledge, the HRM has not been evaluated *in situ* in almond.

My objective was to address the following questions: (1) Which sap flow method, or combination of methods, provides the most reliable estimates of canopy transpiration at both high and low flows? (2) Can sap flow be used to assess which soil and atmospheric index best reflects actual dynamics of water demand? and (3) What additional information or understanding can sap

flow provide to help improve irrigation management? To address these questions, I tested three methods of sap flow (HRM, CHPM and DRM) in artificial stems and in live almond trees to identify the best method, and then applied the best method, in conjunction with measurements of θ and Ψ_{stem}, in almond trees growing in a semi-arid Mediterranean environment with strong seasonal fluctuations in plant available water.

2. METHODS

2.1 Field Site

This study took place from June 2016 to October 2017 on twelve almond trees of four cultivars (four Nonpareil, three Aldrich, two Monterey and three Carmel) within a former pruning trial block that is part of a 40.5 ha almond orchard at Nickels Soil Laboratory, near Arbuckle, California (38°57'29.3N, 122°04'37.5W). The orchard is located 89 m above sea level in a climate characterized by hot, dry summers and mild to cold, wet winters. All varieties were grafted on Lovell root stock and planted in 1997 in a north to south row orientation, with a tree spacing of 6.7 m between rows and 4.9 m within rows. The soils are classified as an Arbuckle series with 20% gravel content and a restricting clay layer beneath 60–120 cm of gravelly, loamy sand. The coarse textured soils limit lateral movement and allow for periods of soil water deficits to be assessed due to rapid water depletion rates. The saturated, field capacity and permanent wilting point volumetric water content values for this site were reported as θ = 0.29, 0.16 and 0.08 m^3 m^{-3}, respectively (Andreu *et al*. 1997). Weeds were managed with strip sprayed herbicides and mowing between rows. Ground water for irrigation is supplied to the orchard by the U.S. Bureau of Reclamation Central Valley Project through the local groundwater authority. Microjet sprinklers were situated midway between trees and used to irrigate based on crop specific soil water depletion rates from ET_c calculations using micrometeorology variables measured with the Nickels Pest Cast

weather station tower (maintained by the University of California Agriculture & Natural Resources Statewide Integrated Pest Management Program). At the onset of hull-split, irrigation was reduced by ~20% over the course of two weeks to accommodate access for orchard floor and pest management. Additional reductions took place 4± days prior to harvest to ensure a completely dry orchard floor and to fortify the trees before being mechanically shaken. ET_c was quite high during both periods of reduced irrigation, such that immediate recovery from the deficit irrigation events was unlikely, resulting in drought periods throughout harvest until the nuts were collected from the orchard floor. Each instrumented tree was hand harvested to avoid damage to the sensors.

2.2 Sensor design and construction

A sap flow sensor set consists of three temperature sensor probes and one heater probe, each 4 cm long and 1.27 mm in diameter. Each temperature sensor probe contains a 10 kΩ precision thermistor, (QTI Sensing Solutions, E320) coated in heat sink compound, that is centered 28 mm from the proximal end into an 18-gauge stainless steel tube (McMaster-Carr, 8987K71). A small amount of low-viscosity cyanoacrylate glue was applied to both ends for anchoring the thermistors inside the tubing. The heater probes were constructed by threading and tightly coiling 50 cm of Manganin resistance wire (Goodfellow, CU065822; resistivity = $4.3–4.8 \cdot 10^{-5}$ Ω·cm) through and around a 5 cm long, 25-gauge stainless steel tube (McMaster-Carr, 5560K46). To avoid unwinding, a drop of low-viscosity cyanoacrylate glue was applied to the proximal end of the resulting heater coil before coating in heat sink compound and inserting into an 18-gauge stainless steel sleeve (McMaster-Carr, 8988K48). Each constructed probe was bent at an angle with small pliers at ~5 mm from the proximal end to prevent rotation, and inserted into a custom-milled Delrin plastic base and affixed with epoxy (OMEGA, OB-100-16). The extruding wires were then

soldered to multi-conductor extension cables that connected to an AM16/32a multiplexer controlled by a CR1000 datalogger (Campbell Scientific).

2.3 Sap Flow Probe Installation

Holes for sensor insertion were drilled using a portable drill guide (Kanzawa, K-801) and a steel levelling plate that was strapped to each tree. Sensor sets were installed on both the east and west sides at ~50 cm from the ground in each tree trunk. These azimuths were initially chosen to explain any possible divergence in tangential fluxes attributable to sap velocity differences as a consequence of height and light interception variability among cultivars. One temperature sensor was placed 0.75 cm proximal to (position x_1 = -0.75 cm in Equation 1 below; "upstream" in terms of the usual direction of water flow), and two others at 0.75 and 2.25 cm distal to (x_2 and x_3, "downstream") the heater probe (Fig. 1). Following installation, the entire trunk at each sensor site was wrapped with 60 cm wide heat-reflective bubble insulation to buffer weather and temperature fluctuations. The dataloggers at each site were programed to open a 3 A relay (Crydom, DC60S3-B) every 15 min, triggering a 5 s heat pulse across the heater wires supplied by a 12 V battery across the heater wires. The total resistance of each heater varied from 13 to 15 Ω, resulting in a 48–55 J heat pulse and a peak temperature rise of ~2 °C in the sensor at position x_2. The resultant temperature change at each sensor was determined by half-bridge measurements of each thermistor recorded every 5 or 6 s following each heat pulse (measurement frequency was limited to 0.2 Hz by the multiplexer scan rate.)

2.4 Sap Velocity Calculations

Prior to sap velocity calculations, the initial temperature of each probe was calculated as the average temperature over a 5 s window preceding each heat pulse. To account for drift in

temperature between heat pulses, background T was interpolated between initial temperatures using a natural cubic spline function.

Three methods were used to estimate sap velocity. The heat-ratio method (HRM) calculates the bulk velocity of heat dissipation by sap velocity (V_h, cm h^{-1}) using the ratio of temperature increases (δ_2/δ_1) for the probes at positions x_1 and x_2 (Fig. 2b):

$$V_{\mathrm{HRM}} = \frac{4kt}{2t(x_2 - x_1)} \ln\left(\frac{\delta_2}{\delta_1}\right) 3600 \qquad (1),$$

where δ_1 and δ_2 are the temperature increases (relative to the pre-heat-pulse background; K) for the probes located at positions x_1 and x_2 relative to the heat probe, respectively, t = time after the heat pulse, k = thermal diffusivity (0.00294 cm^2 s^{-1}, derived from López-Bernal *et al*. 2014), and 3600 converts time from seconds to hours.

Heat velocity was also calculated using the compensation heat-pulse method (CHPM), from the time in seconds, t_0, after the heat pulse at which temperature was equal for the upstream probe (at position $-x_1$) and downstream probe (x_3) (Fig. 2a; Swanson 1962):

$$V_{\mathrm{CHPM}} = \frac{x_1 + x_3}{2t_0} 3600 \qquad (2).$$

The double-ratio method (DRM) is an extension of the HRM, in which two velocity estimates (V_{12} and V_{23}) are calculated, each based on a different ratio of temperature increases (Fig. 3a):

$$V_{12} = \frac{2k}{x_2 - x_1} \ln\left(\frac{\delta_2}{\delta_1}\right) \qquad (3), \text{and}$$

$$V_{23} = \frac{2k}{x_3 - x_2} \ln\left(\frac{\delta_3}{\delta_2}\right) + \frac{x_3 + x_2}{2t} \qquad (4),$$

where δ_3 is the temperature rise of the sensor at position x_3. V_{DRM} is calculated as a weighted average of V_{12} and V_{23}, in which the weighting factors are based on the intrinsic measurement uncertainties for each probe (Fig. 3b):

$$V_{\mathrm{DRM}} = \frac{\left(\frac{1}{\sigma_{12}}\right) V_{12} + \left(\frac{1}{\sigma_{23}}\right) V_{23}}{\left(\frac{1}{\sigma_{12}}\right) + \left(\frac{1}{\sigma_{23}}\right)} \cdot 3600 \qquad (5),$$

where σ_{12} and σ_{23} are the intrinsic uncertainties of V_{12} and V_{23}, respectively (Eqns. 6 and 7):

$$\sigma_{12} = \frac{2k}{x_2 - x_1} \sqrt{\frac{1}{\delta_2^2} + \frac{1}{\delta_1^2}} \qquad (6), \text{ and}$$

$$\sigma_{23} = \frac{2k}{x_3 - x_2} \sqrt{\frac{1}{\delta_2^2} + \frac{1}{\delta_3^2}} \qquad (7).$$

Equations 6 and 7 arise from applying propagation of error rules to Equations 3 and 4. Thus, if the intrinsic uncertainty of V_{12} is much larger than that of V_{23}, V_{DRM} will be primarily determined by V_{23}, and vice versa. Equations 6 and 7 show that the intrinsic uncertainty of a given velocity estimate increases approximately in proportion to the inverse of the smaller temperature rise used to calculate velocity. For example, at very high sap velocities, most of the heat from the heat pulse is carried downstream rapidly; thus, little heat diffuses back to the upstream sensor, making δ_1 small and σ_{12} large relative to σ_{23}. In that case, V_{DRM} would be primarily determined by V_{23}. Conversely, under low or reverse velocities, little heat reaches the third (farthest-downstream) probe, making δ_3 small and σ_{23} large, and ensuring that V_{DRM} is determined mostly by V_{12}.

Burgess *et al*. (2001) described errors that can occur in heat-ratio methods from random noise and heat transfer patterns if an appropriate averaging window (i.e., period of time after the heat pulse in which to average several instantaneous estimates of V) is not chosen. Thus, the time

window in which V_{12} and V_{23} are calculated is important. The version of the DRM proposed by Deng *et al*. (2021) averages the calculations of V within varying time windows centered at the point in time at which measurement noise is smallest. Since these projects overlapped and the final calculation methods were not established before the data presented here was expected to report, I chose a different approach that calculated V_{HRM} and V_{DRM} using measurements during a fixed window of time after each heat pulse (60–100 s). Figure 3a demonstrates that both temperature ratios ($\frac{\delta_2}{\delta_1}$ and $\frac{\delta_3}{\delta_2}$) are approximately constant and free of excessive noise within the 60–100 s timeframe following a heat pulse. I thus averaged the temperature measurements within that time window to compute ratios of mean temperature rise ($\frac{\overline{\delta}_2}{\overline{\delta}_1}$ and $\frac{\overline{\delta}_3}{\overline{\delta}_2}$), and then applied these to Equations (3) and (4), respectively.

To correct for zero offsets in calculated velocity caused by probe wounding (assumed to be 1.4 mm in diameter) and misalignment, both wounding and alignment (for a sensor spaced 7.5 mm from the heater) correction factors were estimated using equations given by Burgess *et al*. (2001) during a period in which I could confidently assume the true velocity was close to zero (because both VPD and solar radiation were negligible and the soil was water-saturated), which occurred between 00:00 and 05:00 h on 08 May 2016. These correction factors were applied during all initial calculations of V (Swanson and Whitfield 1981; Burgess *et al*. 2001). Since *P. dulcis* is a semi-ring-porous species, with variable sapwood anatomy (Scholz *et al*. 2013; López-Bernal *et al*. 2014), the functional sapwood depth can differ greatly around the circumference of a trunk, making it effectively impossible to accurately scale point estimates of sap velocity to whole-tree flow rates. Thus, I did not attempt to scale up sap velocity, and instead averaged V for both probe sets in each tree and normalized the resulting values to produce a relative index (normalized sap velocity, NV; see *Data Analysis* for further details).

2.5 Additional Measurements

Volumetric soil water content (θ) was measured using Frequency Domain Reflectometry soil moisture sensors (Decagon, 10HS) that were installed at 20 and 60 cm depths within the irrigation zone of each tree and the middle of each row, then averaged for each section prior to analysis. Measurements of Ψ_{stem} were taken between 12:00 and 14:00 h every 7 to 10 days with a Scholander pressure chamber (Soilmoisture Equipment Corp.; SAPS II, 3115). Two lower canopy intact leaves per tree were placed in small reflective sleeves with a Velcro enclosure to prevent transpiration, and allowed to equilibrate for at least 10 min before excision to determine plant water status. Measurements of the incoming shortwave solar radiation (R_s; Li-Cor, LI-200R), wind speed (u_2; R.M. Young Company, Wind Sentry 03002), temperature and relative humidity (°C and RH) were obtained simultaneously from sensors (Vaisala, HMP60) that were positioned on a 7 m tall steel pole erected above the canopy of the measured trees.

Hourly ET_{ref} was calculated following the American Society of Civil Engineers (ASCE) Standardized Evapotranspiration guidelines after adjusting for the height at which wind speeds were measured (Eqn. B.14, ACSE*b* 2005) using the "Standardized Reference Evapotranspiration Equation" (Eqn. 1, ASCE*a* 2005),

$$ET_{\mathrm{ref}} = \frac{0.408\,\Delta\,(R_{\mathrm{n}} - H) + \gamma\,\left(\frac{C_{\mathrm{n}}}{T + 273}\right) u_2 (e_{\mathrm{s}} - e_{\mathrm{a}})}{\Delta + \gamma\,(1 + C_{\mathrm{d}} u_2)} \qquad (8),$$

where ET_{ref} is reference evapotranspiration (mm h^{-1}), 0.408 m^2 mm MJ^{-1} is the reciprocal of the latent heat of vaporization (2.45 MJ kg^{-1}) in volumetric units, Δ is the slope of saturation vapor pressure curve (kPa $°C^{-1}$) at the hourly mean air temperature (T, °C), R_n is net shortwave solar radiation at the crop surface (MJ m^{-2} h^{-1}), H is soil heat flux density (MJ m^{-2} h^{-1}), u_2 is wind speed (m s^{-1}), e_s and e_a are saturation and actual vapor pressures, respectively (kPa), γ is the

psychrometric constant (kPa °C^{-1}), and C_n and C_d are the crop roughness and resistance factors, respectively, taken from Table 2 in Appendix A of (ASCE*b* 2005). VPD of the air was calculated as $e_s - e_a$. Crop specific evapotranspiration rates ET_c were calculated as a product of the resultant ET_{ref} values and the corresponding crop coefficients for almonds (K_c; Shackel and Doll 2015).

2.6 Gravimetric flow comparisons

I validated each sap flow method with direct gravimetric flow comparisons on a sand filled pipe. This enables a wider range of flow rates than is possible when forcing water through excised stems in a laboratory, while also allowing direct determination of thermal diffusivity used in the HRM and DRM. A 1 m long and 5 cm diameter PVC pipe partially filled with sand, (lacking fine particles), was capped with a compression gland fitting to secure extended tubing equipped with valves for flow control. The dry bulk density (ρ_b = 1.92 g cm^{-3}) and volumetric moisture content (θ = 45%) of the sand was used to determine the thermal conductivity (K = 5.03 W m^{-1} K^{-1}) and thermal diffusivity ($k = 7 \times 10^{-3}$ cm^2 s^{-1}) after van Wijk and de Vries (1963). A constant head of water was applied to one end and water flows through the pipe and tubing were then measured gravimetrically. Heat pulses were initiated in 10 min intervals for 50 min cycles for each of nine different water fluxes from 0–149 cm^3 cm^{-2} h^{-1}, and each cycle was bookended with 5 min each of maximum flow (valves fully open) and no flow (valves entirely closed) to impede development of tortuous flows. Calculations of sap velocities from each method (DRM, HRM and CHPM) were then compared to the measured water fluxes.

2.7 Data Analysis

Three trees were omitted from data analysis due to poor sensor quality in one Nonpareil tree and substantial extra sun exposure due to tree loss in rows adjacent to two of the instrumented Carmel

trees. All calculations performed on raw sap flow temperature sensor data and all statistical analyses were carried out in R (R Development Core Team, 2020) with specific packages denoted in text. In some analyses, measurements for which R_s was below 50 MJ m^{-2} h^{-1} were excluded to ensure light was adequate to maintain open leaf stomata. To understand the various methods used for determining ET_c, daily means were calculated both with and without nighttime values to expose any possible unexplained relationships that can occur between nocturnal NV and environmental variables.

Normalized isothermal canopy conductance (NG) was calculated by dividing V by VPD to give isothermal canopy conductance (G), and then normalizing the result to its own range (i.e., NG = $[G - \min\{G\}]/[\max\{G\} - \min\{G\}]$). For most analyses, sap flow was likewise normalized to its own range to give normalized sap velocity (NV). These ranges consider the ratio of leaf area to cross sectional area of conducting xylem to be constant, implying the fluctuations in total resistance and conductance are also uniform (Fernández *et al*. 2006).

The relationships between NV and θ, ET_c and Ψ_{stem} under both high and low ranges of values for each variable were assessed with ordinary least squares linear regression. Analysis of variance was used to assess to responses of NV to θ and ET_c; cultivar interactions were found to be statistically insignificant, so values were averaged across all trees. Outliers were detected and omitted using the 'rstatix' package. The dependence of NV on θ and the components of ET_c (VPD, R_s, and u_2) was assessed by multiple linear regression; insignificant predictors were excluded and Akaike's Information Criterion (AIC) used to determine the most parsimonious model. Edward's partial coefficients of determination were calculated for the relationships between NV and each environmental variable in the chosen model using the 'asbio' package. A final examination, using

the 'FactoMineR' package, involved a multivariate analysis to compute Pearson correlation coefficients for all related explanatory variables to the overall trends in both NV and NG.

3. RESULTS

3.1 Sensor validation

Sap velocity calculated using the DRM was linearly related to fluxes measured in the sand-filled PVC pipe, with a slope close to 1 (Fig. 4). The CHPM and HRM velocity estimates were also linearly related to true flux, but with shallower slopes (0.49 and 0.08, respectively), and in the case of CHPM, a large positive intercept (36.5 $cm^3\ cm^{-2}\ h^{-1}$ = $cm\ h^{-1}$). Thus, when the true water flux was zero, the DRM and HRM both computed velocities near zero (-0.8 and -1.0 $cm\ h^{-1}$, respectively), while the CHPM overestimated the velocity as 36.5 $cm\ h^{-1}$. The DRM performed well across a wide range of velocities, from zero to extremely high velocities exceeding those typically observed in almond trees (> 100 $cm\ h^{-1}$), while the HRM and CHPM both underestimated high velocities, and the CHPM overestimated low velocities. For example, the DRM calculated a velocity of 81.5 $cm\ h^{-1}$ when the true velocity was 80 $cm\ h^{-1}$, whereas velocities of 7.8 and 77.1 $cm\ h^{-1}$ were estimated by the HRM and CHPM, respectively (Fig. 4). The fit (as correlation coefficient) of a linear regression of measured vs calculated velocities was best for the DRM followed by the CHPM and HRM, all with high coefficients of determination (r^2 = 0.99, 0.92, 0.83), respectively.

3.2 Performance of sap flow methods in situ at Nickels

At high transpiration rates (above ~20 $cm\ h^{-1}$), sap velocity estimated by the DRM and CHPM corresponded closely, whereas at low transpiration rates (below ~10 $cm\ h^{-1}$), sap velocity estimated by the DRM and HRM agreed (Figs. 5b and 5d); all three methods agreed reasonably well only

for a narrow intermediate range of velocities between ~10 and ~20 cm h^{-1}. For low velocities, the CHPM did not produce meaningful output; for high velocities, the HRM produced meaningful output, but greatly underestimated the velocities reported by the DRM and CHPM (Figs. 5b and 5d). These results, combined with the validation experiments shown in Figure 4, suggest that the DRM was the most reliable of the three methods across a wide range of velocities. This reliability resulted from the DRM assigning greater weight to the more reliable of two heat-ratio-based velocity estimates (V_{12} and V_{23}; Eqns. 3 and 4) based on their respective intrinsic measurement uncertainties. For example, the uncertainty of V_{23} (σ_{23}) was very large in early morning, late afternoon and at night (black lines in Figs. 5a and 5c), whereas the uncertainty of V_{12} (and therefore of V_{HRM}, which is equal to V_{12}) was very large at mid-day (blue lines in Figs. 5a and 5c). All subsequent analyses were therefore performed using sap velocity estimates based on the DRM.

3.3 Relationships between normalized sap velocity, canopy conductance, crop ET, soil water content and stem water potential

Figure 6 illustrates patterns of normalized sap velocity (NV) and normalized isothermal canopy conductance (NG) estimated with the DRM, for an illustrative tree. Strong responses of both NV and NG to changes in both θ and evaporative demand are evident within the grey box of Figure 6 (August 2016), when irrigation was reduced for harvest. During this period, NG and NV declined in response to low θ (indicating stomatal closure), whereas ET_c remained relatively constant. Figure 6 also demonstrates the potential for continuous measurements of NV and NG to capture large variations in tree function that are not detectable either by ET_c (which cannot account for the effect of fluctuations in θ) or by Ψ_{stem} (which cannot practicably be measured at high frequency by growers). For example, during late June through late July, daily maximum NV cycled with a period of roughly one week, between a low of 0.4–0.5 to a high of 0.75–1.0; these large fluctuations were

not evident in daily maximum normalized ET_c, which never fell below 0.75 during this period, nor in measurements of Ψ_{stem}, which remained in a narrow range of -1.1 to -1.5 MPa. These fluctuations in NV were apparently driven largely by stomatal opening and closing (reflected in fluctuations of NG) in response to fairly small variations in soil water content between successive irrigation events. These data indicate a strong and immediate coupling of tree water use to soil moisture. They also show that NG is a far more sensitive and immediate indicator of tree water stress than Ψ_{stem}. For example, during the harvest stress period, NG declined rapidly from ~0.95 to ~0.13, while Ψ_{stem} declined from -1.9 to -2.6 MPa, and failed to detect a partial recovery of stomatal opening in the last week of August (Fig. 6).

Pearson product-moment correlation coefficients were computed to assess the relationships between NV and other variables commonly used to inform irrigation scheduling (Ψ_{stem}, ET_c and θ), under each of the following conditions: high and low ranges of θ and ET_c and high and low values of Ψ_{stem}. The results (Table 1) show positive and significant relationships between NV and each variable, except for a negative relationship with Ψ_{stem} under high Ψ_{stem} values. The strongest relationship (r = 0.72) was that between NV and θ under low θ, followed by the relationship between NV and Ψ_{stem} at low Ψ_{stem} (r = 0.46). These results also revealed that ET_c was a fairly poor predictor of NV, with Pearson coefficients of 0.38 and 0.41 under high and low ET_c, respectively.

To determine whether the ability of ET_c to predict NV improved when data were averaged over each day, I used a linear regression model of daily means for both variables, either including or excluding nocturnal values at high and low θ, and excluding data for the harvest stress period. The slope and tightness of the relationship between NV and normalized ET_c differed between conditions of low and high θ, whether nocturnal data were included (Fig. 7a) or excluded (Fig.

7b): the slope and coefficient of determination were both much larger under high θ (slope = 0.73 and R^2 = 0.69) than low θ (slope = 0.06 and R^2 = 0.01).

To determine whether inclusion of stem water potential could make the relationship between ET_c and NV robust to wide variation in soil moisture, I tested a model of NV as a function of ET_c and Ψ_{stem}^2. Ψ_{stem} was transformed along its range of measured values to account for the upper limit saturation. This model performed well in 2016 under both high and low ranges of ET_c (R^2 = 0.75 and 0.71, respectively; Fig. 8a), but the same form of model performed quite poorly in 2017 (R^2 = 0.38 and 0.15, respectively), and the coefficients for the best-fit model differed greatly between years (Fig. 8b). These results suggest that neither ET_c nor Ψ_{stem} alone, nor both combined, can reliably predict water demand in almond.

3.4 Evapotranspiration components and sap velocity

To determine whether ET_c was itself the best model for predicting NV on the basis of the major meteorological variables underlying ET_c (evaporative demand [VPD] and irradiance [R_s]), I tested a multiple linear regression model of NV vs normalized VPD and irradiance, using daily means calculated with and without nocturnal values. The results differed from the model of NV vs ET_c in two important ways. First, the overall fit of the best model was improved, from R^2 = 0.67 (for NV vs normalized ET_c) to R^2 = 0.79 (for NV vs NVPD and NR_s; Fig. 9a). Second, including nocturnal data increased, rather than decreased, the proportion of variance explained by the latter model (R^2 = 0.59 vs 0.79 if nocturnal data were excluded or included, respectively). Predictions improved further with the addition of normalized soil moisture content (Nθ) as a predictor (Fig. 9b), increasing the proportion of explained variance to 89%. This model also revealed sap velocity was most strongly driven by θ and R_s (a 10% change in Nθ or NR_s resulted in similar changes to NV, 6.1% and 5.6%, respectively) while the same change in NVPD had a much smaller influence

on NV. However, results from both models indicated greater sensitivity to the effects of VPD when Nθ is included as a predictor of NV is more sensitive to 1.7% vs 2.2%). These results indicate that, as a model of tree water use, ET_c overlooks certain effects of environmental variables on actual transpiration, perhaps because ET_c does not explicitly consider responses of stomata to these variables.

3.5 Normalized canopy conductance and its dependence on environmental parameters

To detect the contribution of stomatal movements, I separated the biological component of responses of sap velocity to the environment from the effects of atmospheric demand (VPD) by calculating normalized isothermal canopy conductance (NG). Because NG is controlled mainly by the influences of stomatal opening and closing, and by changes in aerodynamic conductance due to wind, the behavior of NG largely reflects stomatal responses to VPD, R_s and soil moisture. In an illustrative tree (Fig. 10), NG rose with R_s early in the day, whereas NV lagged behind the diurnal rise and fall of R_s, due to the diurnal pattern of VPD, which tended to rise slowly over the day and peak shortly before nightfall. On days 158 and 159 (early June), NG declined earlier than NV in the afternoons due to the continued rise in VPD, partly dampening the positive effect of VPD on NV. NV remained high after R_s reached its maximum, declining only in late afternoon, after the time of peak VPD (Fig. 10a). During water-limited conditions (days 230–232, mid–late August), water stress (which was exacerbated by higher VPD) manifested as large declines in both NV and NG (Fig. 10b). This was observed in all three cultivars and in both 2016 and 2017 (not shown here).

NG was driven strongly by radiation, but was less influenced by wind speed (Figs. 11a and c). The relationship between NG and wind speed was very weak at all times of the day and night

(maximum correlation values, $r = 0.2$, were obtained at night and when NG was increasing in the morning). Conversely, the relationship between NG and radiation was strong ($r = 0.6$) whenever R_s was changing rapidly (either increasing in the morning or decreasing in the late afternoon). The response of NG to wind speed was negative at night, and also at midday under low θ, contradicting the expected effect of wind on the aerodynamic component of canopy conductance. This likely represents local inversion-like conditions, in which clear skies, low temperatures and low wind speeds drive stomatal opening by reducing VPD (Fig. 11b).

I used a linear regression model to assess the relationship between midday NG and Ψ_{stem}, and related the residuals to other environmental variables to determine if and why Ψ_{stem} fails to predict declines in midday NG. Results revealed positive relationships between the residuals of this model and each of wind speed (Fig. 12c), solar radiation (Fig. 12b) and soil moisture (Fig. 12a), demonstrating that Ψ_{stem} alone cannot reliably predict changes in canopy conductance. Replacing Ψ_{stem} (Fig. 13a) with soil moisture (Fig. 13b), or combining both (Fig. 13c), did not substantially improve predictions of NG, suggesting that Ψ_{stem} and θ contain similar information about the environmental control of canopy conductance.

4. DISCUSSION

As water becomes more scarce there is a growing need for plant-based methods for irrigation scheduling that can complement existing methods. In particular, current methods cannot capture diurnal dynamics of transpiration patterns and are difficult to integrate with current understanding of how plants respond physiologically to water deficit. This study has focused on the utility of sap flow methods to fill this gap. Sap velocity can provide two types of information that have the potential to be useful in irrigation scheduling: estimates of variations in water use and thus water demand (from normalized sap velocity itself) and estimates of the manifestation of water stress at

the canopy level (from normalized canopy conductance, which mainly reflects stomatal opening and closing). My results suggest that ET_c is a reasonable predictor of day-to-day variation in actual water use, but that its accuracy depends sensitively on soil moisture, even during periods of regular irrigation. Furthermore, ET_c was outperformed as a predictor of tree water use by a simple linear model combining radiation, VPD and soil moisture. These results suggest that, (1) as a model for predicting water demand, ET_c omits some significant responses of transpiration to the environment, likely driven by variations in canopy conductance due to stomatal opening and closing, and that (2) sap flow has the potential to identify and help to explain these gaps, and thereby to complement, inform and improve ET_c and other current irrigation scheduling methods. I also found that a novel sap flow methodology, the dual-ratio method or DRM, is suitable for measuring the wide range of rates that occur in almond, and outperforms other current pulse-based methods.

4.1 Sap flow methodologies

My results suggest that the DRM sap flow methodology (Deng *et al*. 2021) can accurately detect both very low and very high sap velocities, overcoming the HRM's inability to measure high velocities. This is achieved by computing a weighted average of two different estimates of sap velocity, one of which is more robust at low rates and the other at high rates. Pearsall *et al*. (2014) suggested a similar approach, wherein the HRM was used at low flow rates and the CHPM at high flow rates. Earlier studies had found that the CHPM is unreliable at low velocities, and that the HRM becomes insensitive to increasing rates above approximately 15 to 35 cm h^{-1} (Bleby *et al*. 2004; Pearsall *et al*. 2014). The DRM has two advantages over the method suggested by Pearsall *et al*. (2014). First, the influence of measurement noise is reduced by not relying on a single instantaneous measurement, as the CHPM does. Second, the DRM’s error-based method to weight

the two velocity estimates does not require the user to specify an arbitrary velocity value at which to switch from one estimate to another. Nevertheless, both the DRM and the Pearsall method show that sap velocity can be accurately measured across a very wide range of rates using pulse-based techniques. The results presented here extend that finding to almond trees. The DRM was able to measure higher sap velocities than the HRM, and lower velocities than the CHPM, both in validation experiments in a tube filled with sand under controlled flow, and in almond trees. Thus, the DRM has potential to be useful in crops like almonds, in which sap velocities vary from high to low extremes diurnally and seasonally in relation to water stress.

4.2 How well do ET_c or its individual components predict sap velocities?

While ET_c predicted sap flow reasonably well in well-watered conditions, as expected ET_c was a less reliable predictor under mild soil water deficit as θ approached 0.14 $m^3 m^{-3}$. NV was able to detect reductions of transpiration by both moderate declines in θ during brief (3-8 day) intervals between irrigation events, and larger declines in θ during extended water stress associated with water cutbacks associated with harvest. ET_c could not, by design, predict these declines in NV, because ET_{ref} methods are formulated for conditions when water is not limiting, and lookup tables for K_c are not intended to accommodate declines in θ between successive irrigation events. Nevertheless, even under conditions of high soil moisture, ET_c could only predict, at most, two-thirds of variation in daily total sap velocity (Fig. 8b). This is likely due, at least in part, to biological responses involved in canopy conductance, and perhaps endogenous factors that affect stomata, such as hydraulic conductance, which can vary over time and across environments and are not captured by ET_c calculations.

I found that predictions of sap velocity could be greatly improved – reducing unexplained variance in NV by more than a third – using a simple linear model of the two main meteorological

drivers of ET_c (radiation and VPD; Fig. 9a). Adding soil moisture as a predictor cut the remaining unexplained variation by half, leaving only 11% of variance unexplained by the model (Fig. 9b). These results illustrate the importance of taking VPD into account when determining water use in almonds, as illustrated by the response rate of NG to diurnal fluctuations in plant water status (Figs. 6 and 10) and as previously noted by Shackel *et al*. (2010) in relation to calculating baseline water potentials for almonds. They also raise questions about the accuracy and efficacy of the ET_{ref}/K_c-based model for irrigation scheduling. If a model ostensibly based on atmospheric physics and biology (ET_{ref} and K_c) performs more poorly than an uninformed linear model of the underlying variables, then it may be worth revisiting the ET_c paradigm. In this context, sap flow techniques such as the DRM or the method of Pearsall *et al*. (2014) can be useful research tools for improving the empirical and physiological basis of irrigation scheduling methods. If used in conjunction with integrated flux measurements such as surface renewal or eddy covariance (Cammalleri *et al*. 2013), sap flow can also help to separate soil evaporation from canopy ET (because sap flow reflects only the latter), as well as clarify the contribution of nocturnal transpiration (which is often poorly estimated by above-canopy flux approaches; Fisher *et al.* 2007). I found small but nontrivial rates of sap flow at night (e.g., Figs. 5 and 6).

4.3 Potential sources of error in ET_c calculations

There are numerous reasons for which ET_c might diverge from actual canopy ET, even under conditions of high soil moisture. For instance, most methods use a set solar angle at night to ensure ET_c values are at or near zero, whereas real canopies may continue transpiring significantly at night. Additionally, the Penman-Monteith equation strictly requires knowledge of canopy-averaged leaf surface resistance (which includes an important contribution by stomatal resistance) as an input; this resistance is usually treated as an input constant in calculating ET_{ref}, but in reality

stomatal resistance varies greatly over a day, and even from day to day as VPD, irradiance and soil moisture differ (e.g., Figs. 6 and 10; Irmak *et al.* 2005). Finally, other parameters used in calculating ET_{ref} are variable in actuality but are usually applied as constants, including aerodynamic resistance, crop height, albedo and soil heat flux, each of which can fluctuate at time scales ranging from hourly to seasonally (Irmak *et al.* 2005, Allen *et al.* 2010). The identification of the proper crop coefficient multiplier (K_c) is another potential source of error in ET_c calculations. Researchers have determined a variety of seasonal K_c values (Doll 2020). However, these values cannot resolve for spatial variability in orchard or individual tree ET caused by differences in soil composition, drainage, distribution, or management practices. Thus, any worthwhile improvements in ET_c calculations would require updated K_c values that consider such disparities.

4.4 Optimizing crop water use and supply with canopy conductance

Normalized isothermal canopy conductance (NG) provided additional, and potentially useful, information about the physiological status of almond trees in relation to water stress, beyond that provided by normalized sap velocity (NV). The greatest value of NG is in identifying water stress that coincides with an increase in VPD. For example, if soil moisture is becoming low enough as to require additional irrigation inputs, this would manifest in a reduction of NG; however, if VPD happened to be elevated during such conditions, then NG would decline further, whereas NV would generally increase or remain nearly constant, thus masking the emerging water stress. Although Ψ_{stem} can provide similar information as NG about the occurrence of water stress, NG has the advantage of being a continuous measurement, whereas it is typically not practical for growers to measure Ψ_{stem} daily, let alone at sub-hourly resolution as is possible with sap flow-based NG.

NG also has value in the context of research to improve the knowledge basis of irrigation scheduling methods. For one, it can help clarify the role of aerodynamic coupling between the canopy and atmosphere in the regulation of ET in almond. In this study, NG was weakly related to wind speed under most conditions, which likely indicates that aerodynamic resistance was generally small relative to stomatal resistance – consistent with some previous results in almond (Granier 2000), but not others (Spinelli *et al*. 2017). Additionally, NG can be combined with *in situ* measurements of leaf stomatal conductance and photosynthetic responses to model canopy photosynthesis, providing an important added dimension to the physiological rationale behind irrigation management (e.g., Fernandez *et al*. 2006, Fernandez *et al*. 2008, Egea *et al*. 2011, Diaz-Espejo *et al*. 2012).

The escalating concerns in global water security and more accessible technologies have increased research interests in exploring the use of canopy conductance as an indicator for crop water requirements. My results suggest that this approach could be used not only to improve prediction and quantification of ET, but also to detect stress in plants in order to trigger the timing of irrigation events. If the significance of a 0.3mm d^{-1} over- or underestimation of ET_{ref} (equivalent to a difference of 3 m^3 ha^{-1}) were given more consideration on a watershed to regional scale, emphasis on more precise irrigation estimations would be appreciated (Irmak *et al*. 2005). Studies have shown that even mild to moderate water stress in almonds results in adverse yield and health effects (Doll 2014). The additional insight into the dynamics of stomatal conductance and photosynthesis provided by canopy conductance may prove valuable in the future for the agricultural sector (Jones 2004). Interestingly, it has been over a decade since estimations of canopy conductance from sap flow measurements were collected on three tree crops (orange, olive and plum) with reports of promising results (Diaz-Espejo *et al.* 2009). However, as with any

physiological decision support tool aimed at providing a universal answer, further studies across multiple species with additional measurements, such as canopy temperature or stem moisture content, will aid in expediting a much needed reliable irrigation indicator method.

5. CONCLUSION

In situ sap velocity measurements and gravimetric flow experiments clearly indicated that the DRM was more capable of resolving both high and low sap velocities than the HRM or CHPM. Micrometeorology, soil water content, and sap flow measurements over the course of two growing seasons revealed that sap flow measurements can reliably detect water stress in almonds. Sap flow may also be useful for refining current methods of estimating ET. However, although sap flow is excellent for quantifying relative transpiration rate and its diurnal dynamics, it is generally impractical for quantifying absolute transpiration; its main utility in irrigation scheduling arises from the ability to quantify water stress at high time resolutions via the derived parameter of normalized canopy conductance, and from the ability to identify weak points in the calculation of ET_c by standard methods. Future work should aim to develop this potential by coupling sap flow measurements with a variety of simultaneous physiological parameters, including stem water potential and leaf or canopy temperature, across various tree crops to fully characterize the underlying mechanisms responsible for temporal and spatial variations in plant water status of irrigation intensive tree crops.

REFERENCES

Allen, R. G., Pereira, L. S., Raes, D., and Smith, M. (1998). Crop evapotranspiration-Guidelines for computing crop water requirements-FAO Irrigation and drainage paper 56. *FAO, Rome*, *300*(9), D05109.

Allen, R. & Walter, I. & Elliott, R. & Jensen, M. & Itenfisu, D & Howell, T & Snyder, R. & Brown, P & Echings, S. & Spofford, T. & Hattendorf, M. (2011). Issues, requirements and challenges in selecting and specifying a standardized ET equation.

Aho Ken (2020). asbio: A Collection of Statistical Tools for Biologists. R package version 1.6-5. (https://CRAN.R-project.org/package=asbio).

Alboukadel Kassambara (2020). rstatix: Pipe-Friendly Framework for Basic Statistical Tests. R package version 0.6.0. (https://CRAN.R-project.org/package=rstatix).

ASCE-EWRI (2005). The ASCE standardized reference evapotranspiration equation. ASCE-EWRI Standardization of Reference Evapotranspiration Task Committee Rep., ASCE Reston, Va.

Andreu, L., Hopmans, J. W., and Schwankl, L. J. (1997). Spatial and temporal distribution of soil water balance for a drip-irrigated almond tree. *Agricultural Water Management*, *35*(1), 123-146.

Aslyng, H. ~(1965). Evaporation, evapotranspiration and water balance investigations at Copenhagen 1955–64. *Acta Agriculturae Scandinavica*, *15*(3-4), 284-300.

Bleby, T. M., Burgess, S. S., and Adams, M. A. (2004). A validation, comparison and error analysis of two heat-pulse methods for measuring sap flow in Eucalyptus marginata saplings. *Functional Plant Biology*, *31*(6), 645-658.

Burgess, S. S., Adams, M. A., Turner, N. C., Beverly, ~R., Ong, ~K., Khan, A. A., and Bleby, T. M. (2001). An improved heat pulse method to measure low and reverse rates of sap flow in woody plants. *Tree physiology*, *21*(9), 589-598.

[CDFA] California Department of Food and Agriculture (2018). *California Agricultural Statistics Review 2017-2018.* (02 September 2020; https://www.cdfa.ca.gov/statistics/)

[CDWR] California Department of Water Resources (2016). *Agriculture Water Use Efficiency*: *A Resource Management Strategy of the California Water Plan.* (02 September 2020; https://water.ca.gov/California-Water-Plan)

Cammalleri, C., Rallo, G., Agnese, C., Ciraolo, G., Minacapilli, M., Provenzano, G. (2013). Combined use of eddy covariance and sap flow techniques for partition of ET fluxes and water stress assessment in an irrigated olive orchard, *Agricultural Water Management*, 120, 89-97.

Deng, Z., Vice, H., Gilbert, M., Adams, M., Buckley, T. (2021). The double-ratio method (DRM): a robust three-probe sap flow technology that can accurately measure high, low and reverse flows. *Tree Physiology*, https://doi.org/10.22541/au.160029723.31338061

Diaz-Espejo, A. and Fernández, J.E. (2009). Use of sap-flow profiles in trunks to derive canopy conductance. *Acta Hortic*. 846, 271-276.

Díaz-Espejo, A., Buckley, T. N., Sperry, J. S., Cuevas, M. V., De Cires, A., Elsayed-Farag, S., ... & Fernandez, J. E. (2012). Steps toward an improvement in process-based models of water use by fruit trees: a case study in olive. *Agricultural Water Management*, *114*, 37-49.

Doll, D. (2014). Impacts of Drought on Almond Production. (02 September 2020; https://www.growingproduce.com/fruits/impacts-of-drought-on-almond-production/)

Doll, D. (2020). The Almond Doctor. *Almond Irrigation Scheduling: Deciding on a Crop Coefficient.* (18 September 2020; https://thealmonddoctor.com/2020/03/26)

Egea, G., Pagán, E., Baille, A., Domingo, R., Nortes, P. A., and Pérez-Pastor, A. (2009). Usefulness of establishing trunk diameter based reference lines for irrigation scheduling in almond trees. *Irrigation Science*, *27*(6), 431-441.

Egea, G., Gonzalez-Real, M.M., Baille, A., Nortes, P.A. and Diaz-Espejo, A. (2011), Disentangling the contributions of ontogeny and water stress to photosynthetic limitations in almond trees. Plant, Cell & Environment, 34: 962-979.

Espadafor, M., Orgaz, F., Testi, L., Lorite, I. J., and Villalobos, F. J. (2015). Transpiration of young almond trees in relation to intercepted radiation. *Irrigation Science*, *33*(4), 265-275.

Fernández, J.E., Díaz-Espejo, A., Infante, J.M. *et al.* Water relations and gas exchange in olive trees under regulated deficit irrigation and partial rootzone drying. *Plant Soil* **284,** 273–291 (2006).

Fernández J. E., Romero R., Montaño J. C., Diaz-Espejo A., Muriel J. L., Cuevas M. V., Moreno F., Girón I. F., Palomo M. J. (2008) Design and testing of an automatic irrigation controller for fruit tree orchards, based on sap flow measurements. *Australian Journal of Agricultural Research* **59**, 589-598.

Fisher, J.B., Baldocchi, D.D., Misson, L., Dawson, T.E. and Goldstein, A.H. (2007). What the towers don't see at night: nocturnal sap flow in trees and shrubs at two AmeriFlux sites in California. *Tree Physiology*, *27*(*4*), pp.597-610.

Goldhamer, D. A., and Viveros, M. (2000). Effects of preharvest irrigation cutoff durations and postharvest water deprivation on almond tree performance. *Irrigation Science*, *19*(3), 125-131.

Goldhamer, D. A., and Fereres, E. (2004). Irrigation scheduling of almond trees with trunk diameter sensors. *Irrigation Science*, *23*(1), 11-19.

Granier, A. (1987). Evaluation of transpiration in a Douglas-fir stand by means of sap flow measurements. *Tree physiology*, *3*(4), 309-320.

Granier, A., Biron, P., and Lemoine, D. (2000). Water balance, transpiration and canopy conductance in two beech stands. *Agricultural and forest meteorology*, *100*(4), 291-308.

Green, S. R., and Clothier, B. E. (1988). Water use of kiwifruit vines and apple trees by the heat-pulse technique. *Journal of Experimental Botany*, *39*(1), 115-123.

Hernandez-Santana, V., Rodriguez-Dominguez, ~M., Fernández, J. E., and Diaz-Espejo, A. (2016). Role of leaf hydraulic conductance in the regulation of stomatal conductance in almond and olive in response to water stress. *Tree physiology*, *36*(6), 725-735.

Irmak, S., Howell, T. A., Allen, R. G., Payero, J. O., & Martin, D. L. (2005). Standardized ASCE Penman-Monteith: Impact of sum-of-hourly vs. 24-hour timestep computations at reference weather station sites. *Transactions of the ASAE*, *48*(3), 1063-1077.

Johnson, R., Williams, L., Ayars, J., and Trout, T. (2005). Weighing lysimeters aid study of water relations in tree and vine crops. *California agriculture*, *59*(2), 133-136.

Jones, H. G. (2004). Irrigation scheduling: advantages and pitfalls of plant-based methods. *Journal of experimental botany*, *55*(407), 2427-2436.

López-Bernal, Á., Alcántara, E., and Villalobos, F. J. (2014). Thermal properties of sapwood of fruit trees as affected by anatomy and water potential: errors in sap flux density measurements based on heat pulse methods. *Trees*, *28*(6), 1623-1634.

López-Bernal, Á., Testi, L., and Villalobos, F. J. (2017). A single-probe heat pulse method for estimating sap velocity in trees. *New Phytologist*, *216*(1), 321-329.

Marshall, D. ~(1958). Measurement of sap flow in conifers by heat transport. *Plant physiology*, *33*(6), 385.

Nortes, P. A., Baille, A., Egea, G., González-Real, M. M., and Domingo, R. (2008, October). Comparison of almond tree transpiration determined by sap flow measurements and lysimetry. In *VII International Workshop on Sap Flow 846* (pp. 359-366).

Pearsall, K. R., Williams, L. E., Castorani, S., Bleby, T. M., and McElrone, A. J. (2014). Evaluating the potential of a novel dual heat-pulse sensor to measure volumetric water use in grapevines under a range of flow conditions. *Functional plant biology*, *41*(8), 874-883.

Phogat, V., Skewes, M. A., Mahadevan, M., and Cox, J. W. (2013). Evaluation of soil plant system response to pulsed drip irrigation of an almond tree under sustained stress conditions. *Agricultural water management*, *118*, 1-11.

R version 4.0.3 (2020-10-10) -- "Bunny-Wunnies Freak Out" Copyright (C) 2020 The R Foundation for Statistical Computing. Platform: x86_64-w64-mingw32/x64 (64-bit).

Romero, R., Muriel, J. L., and Garcia, I. (2008, October). Automatic irrigation system in almonds and walnuts trees based on sap flow measurements. In *VII International Workshop on Sap Flow 846* (pp. 135-142).

Scholz, A., Rabaey, D., Stein, A., Cochard, H., Smets, E., and Jansen, S. (2013). The evolution and function of vessel and pit characters with respect to cavitation resistance across 10 Prunus species. *Tree physiology*, *33*(7), 684-694.

Sebastien Le, Julie Josse, Francois Husson (2008). FactoMineR: An R Package for Multivariate Analysis. Journal of Statistical Software, 25(1), 1-18. 10.18637/jss.v025.i01.

Shackel, K. A., Johnson, R. S., Medawar, ~K., and Phene, ~J. (1992). Substantial errors in estimates of sap flow using the heat balance technique on woody stems under field conditions. *Journal of the American Society for Horticultural Science*, *117*(2), 351-356.

Shackel, K. A., Buchner, R. P., Connell, J. H., Edstrom, J. P., Fulton, A. E., Holtz, B. A., ... and Viveros, M. A. (2010). Midday stem water potential as a basis for irrigation scheduling. In *5th National Decennial Irrigation Conference Proceedings, 5-8 December 2010, Phoenix Convention Center, Phoenix, Arizona USA* (p. 1). American Society of Agricultural and Biological Engineers.

Spinelli, G. M., Shackel, K. A., and Gilbert, M. E. (2017). A model exploring whether the coupled effects of plant water supply and demand affect the interpretation of water potentials and irrigation management. *Agricultural Water Management*, *192*, 271-280.

Stewart, W., Fulton, A., Krueger, W., Lampinen, B., and Shackel, K. (2011). Regulated deficit irrigation reduces water use of almonds without affecting yield. *California Agriculture*, *65*(2), 90-95.

Swanson, R. H. (1962). Instrument for detecting sap movement in woody plants.

Swanson, R. H., and Whitfield, D. W. A. (1981). A numerical analysis of heat pulse velocity theory and practice. *Journal of experimental botany*, *32*(1), 221-239.

Ullrich, P. A., Xu, Z., Rhoades, A. M., Dettinger, M. D., Mount, J. F., Jones, A. D., & Vahmani, P. (2018). California's drought of the future: A midcentury recreation of the exceptional conditions of 2012– 2017. *Earth's Future*, *6*, 1568–1587.

Vandegehuchte, M. W., and Steppe, K. (2012). Sapflow+: a four-needle heat-pulse sap flow sensor enabling nonempirical sap flux density and water content measurements. *New Phytologist*, *196*(1), 306-317.

Van Wijk, W. R., and De Vries, D. A. (1963). Periodic temperature variation, Physics of Plant Environment WR Van Wijk, 210-235.

Yadollahi, A., Arzani, K., Ebadi, A., Wirthensohn, M., and Karimi, S. (2011). The response of different almond genotypes to moderate and severe water stress in order to screen for drought tolerance. *Scientia horticulturae*, *129*(3), 403-413.

Tables

Table 1 Pearson product-moment correlation was calculated to assess the relationship of normalized sap velocity (NV) to three most commonly used water status indicators, under high and low levels of those indicators.

Response: NV	*r*	*df*	*p*
Low Ψ_{stem}	0.46	91	<.0001
High Ψ_{stem}	-0.20	121	0.03
Low ET_c	0.41	78	0.00
High ET_c	0.38	134	<.0001
Low θ	0.72	68	<.0001
High θ	0.39	144	<.0001

Correlation is significant at the 0.03 level*; two-sided. Stem water potential (Ψ_{stem}), crop evapotranspiration (ET_c), soil water content (θ).

Figures

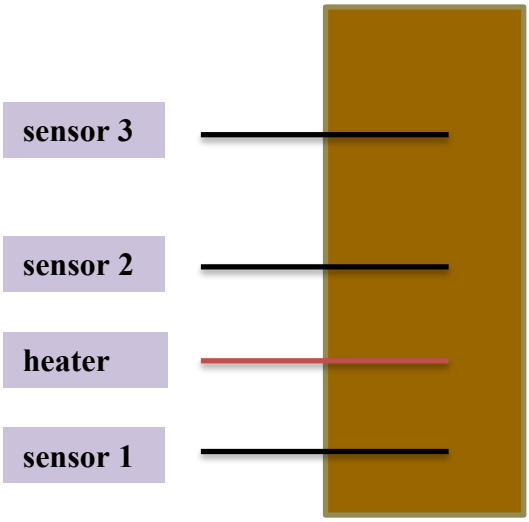

Figure 1. A diagram to illustrate probe placement. Sensor 1 (x_1) is -0.75 cm upstream, and sensors 2 (x_2) and 3 (x_3) are 0.75 and 2.25 cm downstream from the heater, respectively.

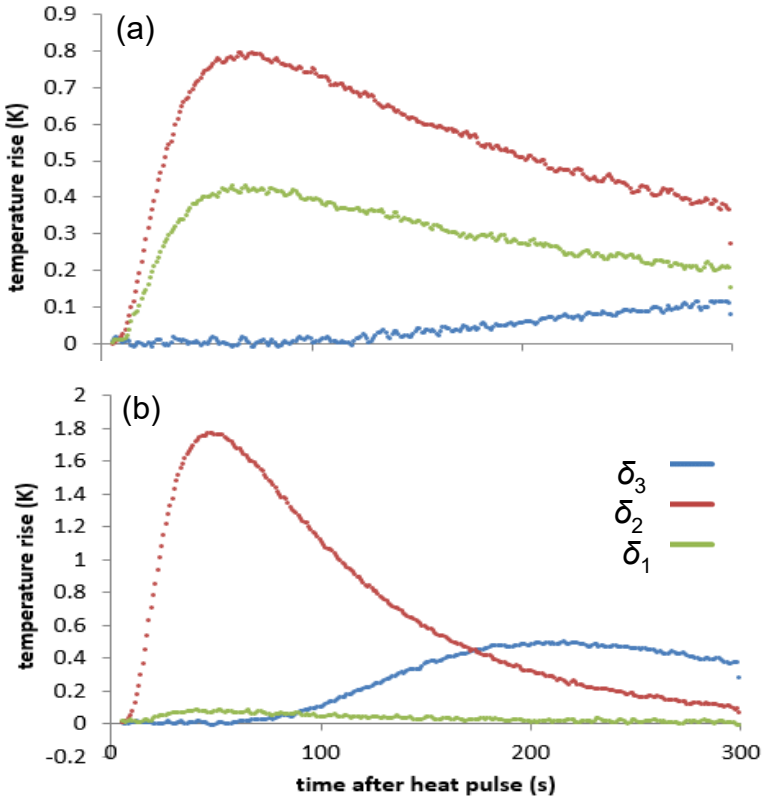

Figure 2. Two illustrative heat pulses, (a) at low transpiration rates demonstrating the absence of an intersection between δ_1 and δ_3 temperature rises that are required for the Compensation Heat Pulse Method calculations, and (b) at high transpiration rates when the prevailing temperature changes from convection cause δ_1 to remain relatively flat resulting in a plateau for the ratio of δ_1 and δ_2 temperature changes, corresponding to the threshold for estimations using the Heat Ratio Method.

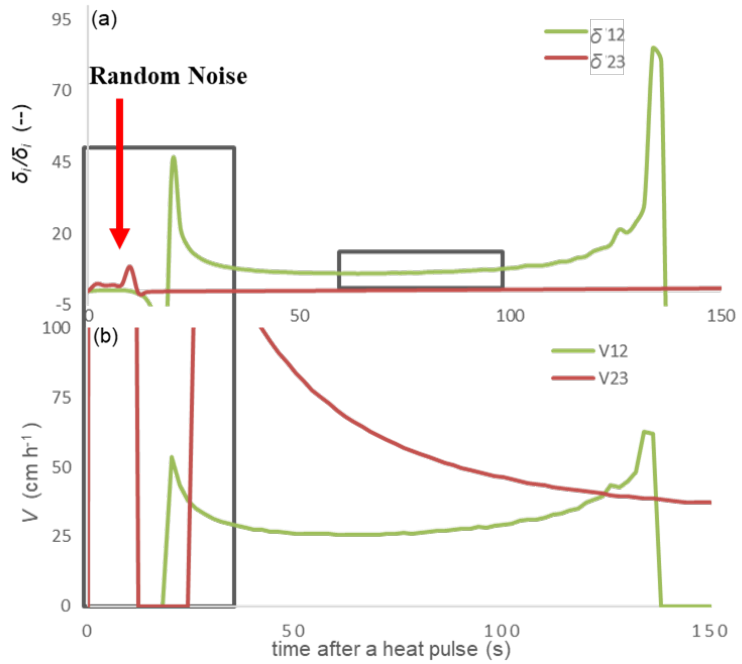

Figure 3. The ratio of temperature rises, δ_2/δ_1 and δ_3/δ_2, between sensors, x_2/x_1 and x_2/x_3, (a) are used to calculate velocities V_{12} and V_{23} (b). The time window in which the ratios are calculated (small box) and traces of the random noise errors that can occur following a heat pulse (large box).

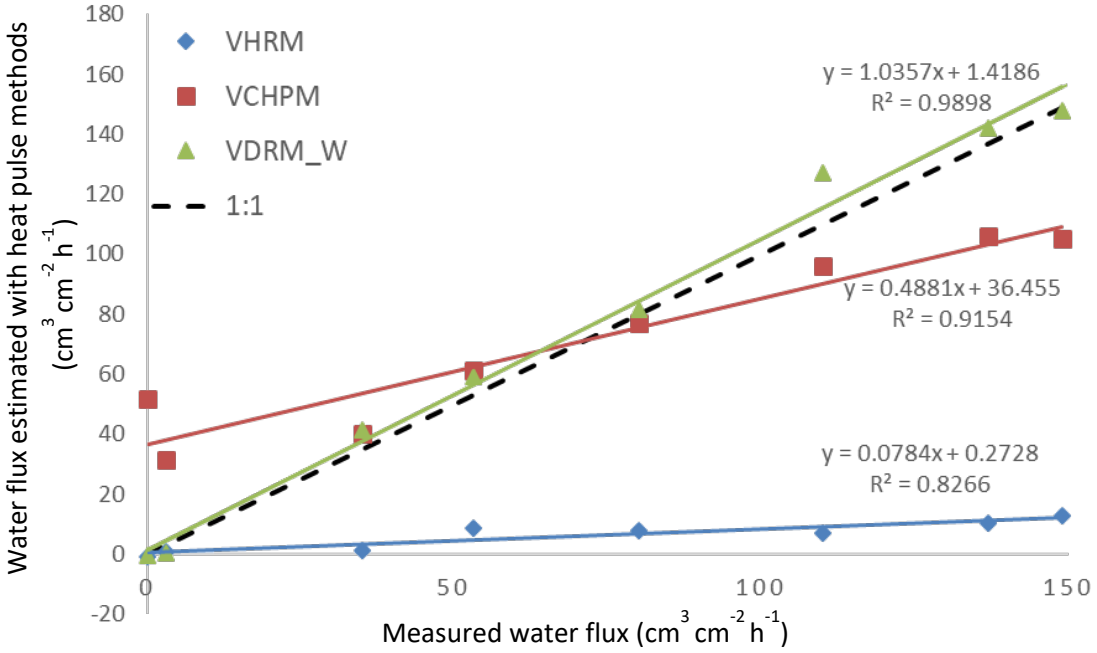

Figure 4. Results of the heat-ratio method (HRM), compensation heat-pulse method (CHPM), and double-ratio method (DRM) performance for calculating true gravimetric water flux in a sand-filled PVC pipe.

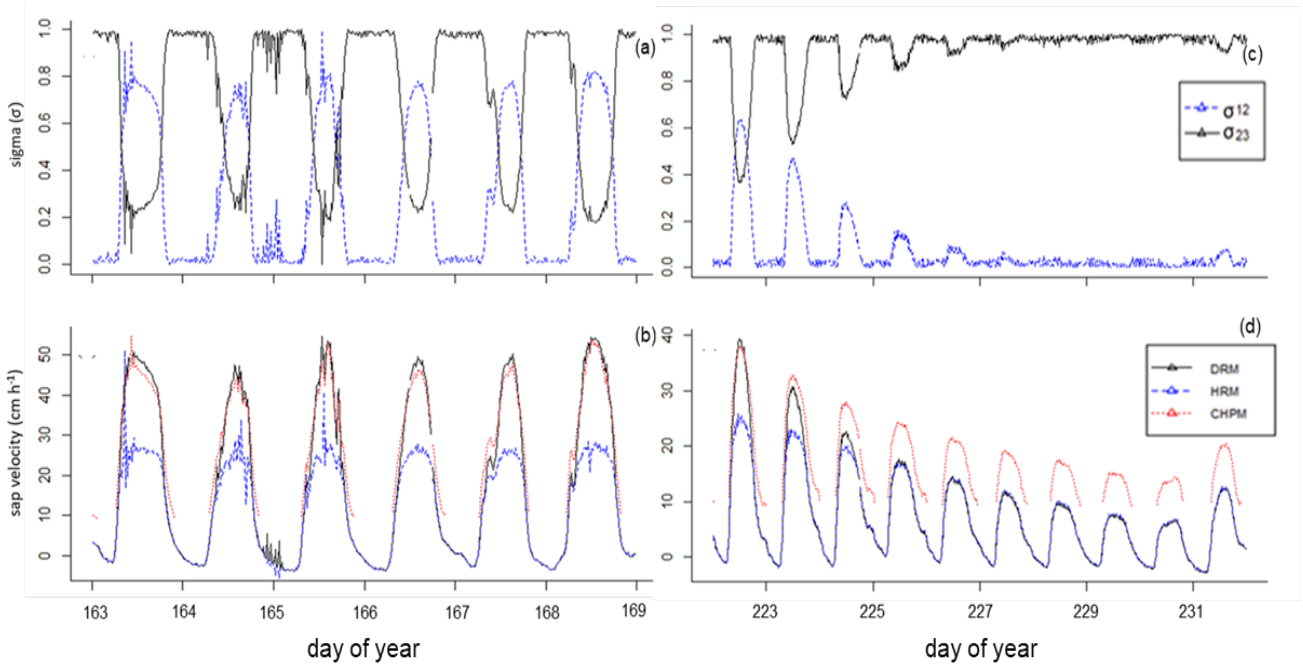

Figure 5. Diurnal patterns of the measurement uncertainties (σ_{12} and σ_{23}) for sensor pairs x_1 and x_2, and sensors x_2 and x_3 (a,c), and sap velocities (b,d) calculated with the double-ratio (DRM), heat-ratio (HRM), and compensation heat-pulse methods (CHPM) during a week of high transpiration when water was not limiting (a,b) and low transpiration during water limited conditions (c,d) in 2016 for an illustrative tree.

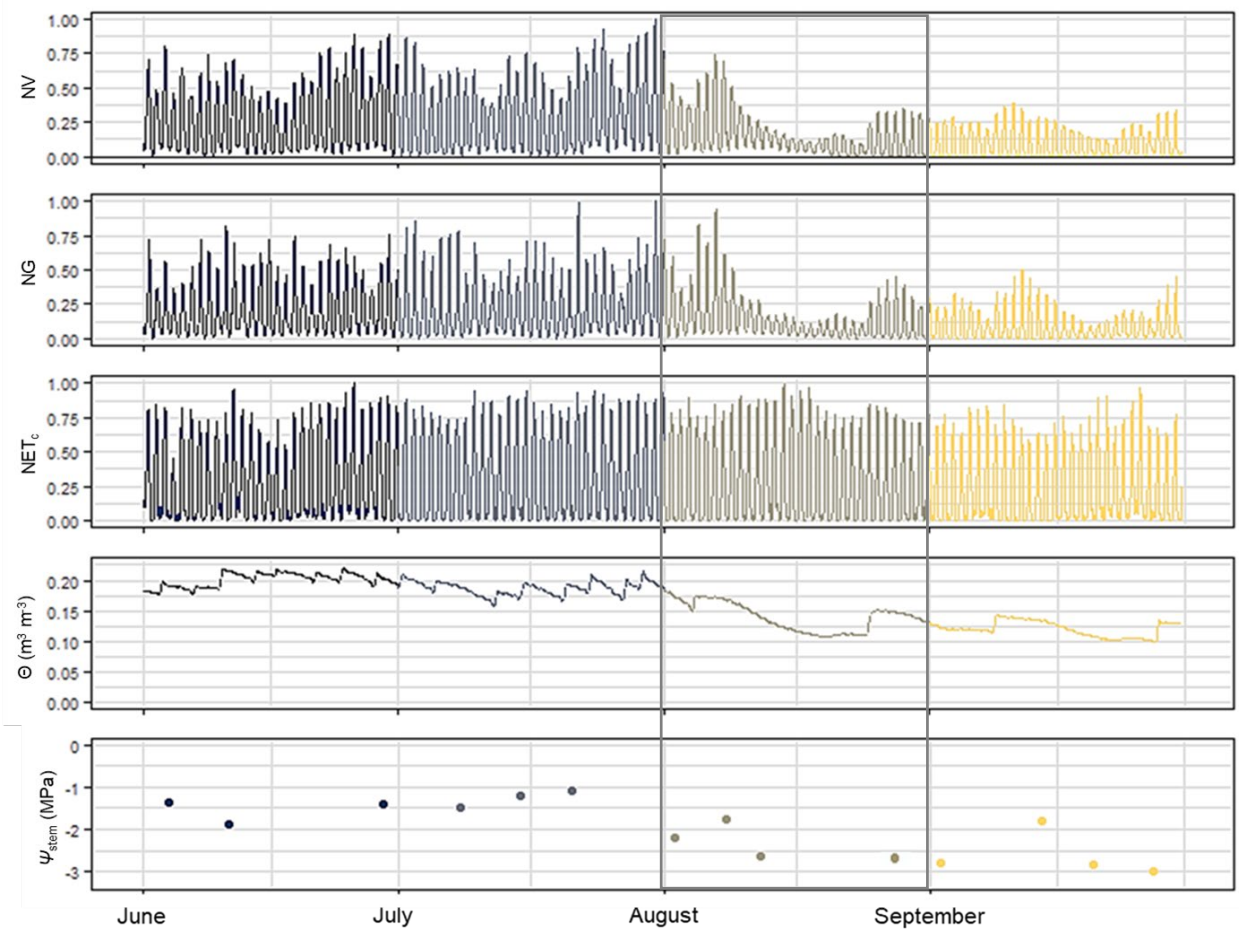

Figure 6. From the top to bottom panels: 2016 seasonal normalized sap velocity (NV) calculated using the double-ratio method, normalized isothermal canopy conductance (NG), normalized crop evapotranspiration (NET_c), soil water content (θ), and midday stem water potentials (Ψ_{stem}) in an illustrative tree at Nickels Soil Laboratory.

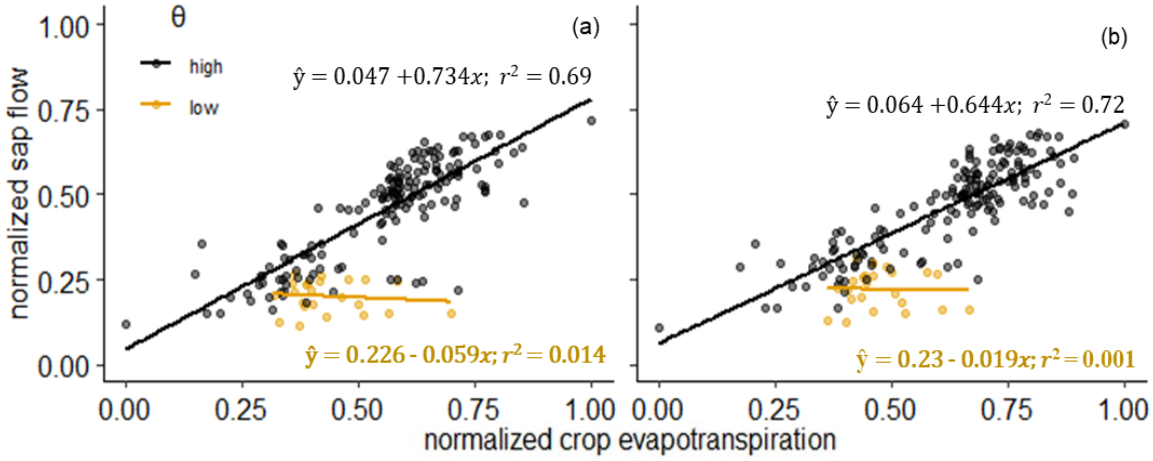

Figure 7. Averaged daily normalized sap velocity, calculated including (a) and excluding (b) nighttime data, as predicted by crop evapotranspiration at high (> 0.14 m^3 m^{-3}, black lines and symbols) and low (< 0.14 m^3 m^{-3}, tan lines and symbols) soil water content (θ) values. Data shown here exclude harvest periods in August.

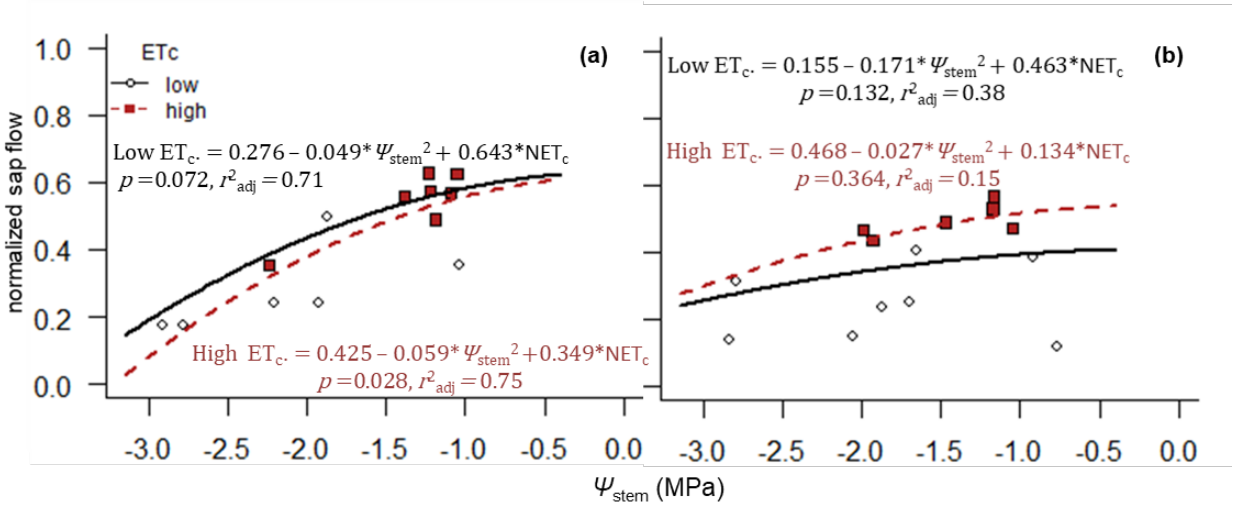

Figure 8. Relationship between midday stem water potential (Ψ_{stem}) and normalized daily sap velocities, under high and low (above or below 6.8 mm d^{-1}, respectively) ranges of crop evapotranspiration (ET_c) for all trees during (a) 2016 and (b) 2017, with corresponding regression model lines. Data are expressed as the mean of all trees per day.

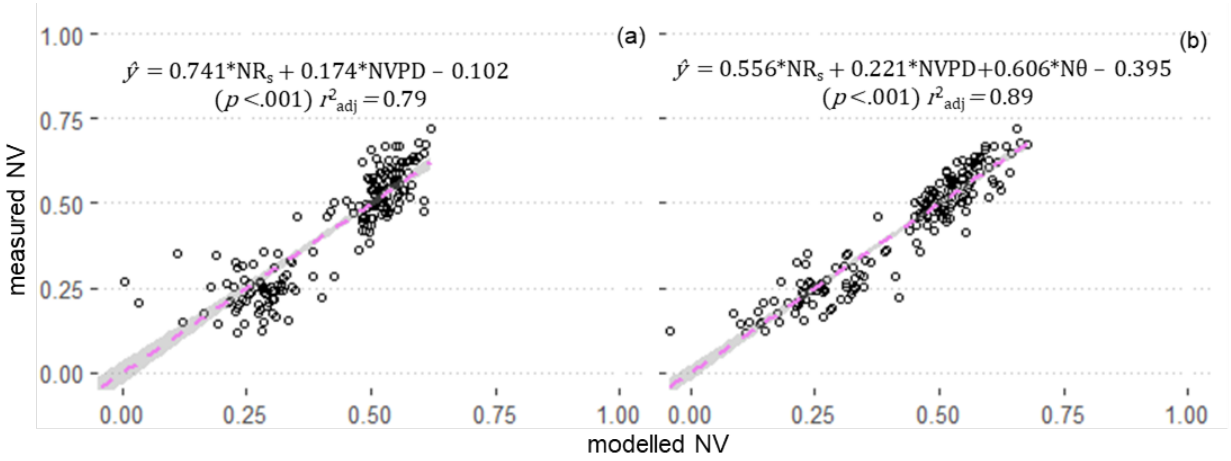

Figure 9. Averaged daily normalized sap velocity (NV) as predicted by (a) the individual components of ET_c (normalized solar radiation, NRs, and vapor pressure deficit, NVPD), and (b) NRs, NVPD and normalized soil water content (Nθ). Data was subset to exclude harvest periods in August and nocturnal data was included in the daily averages shown here.

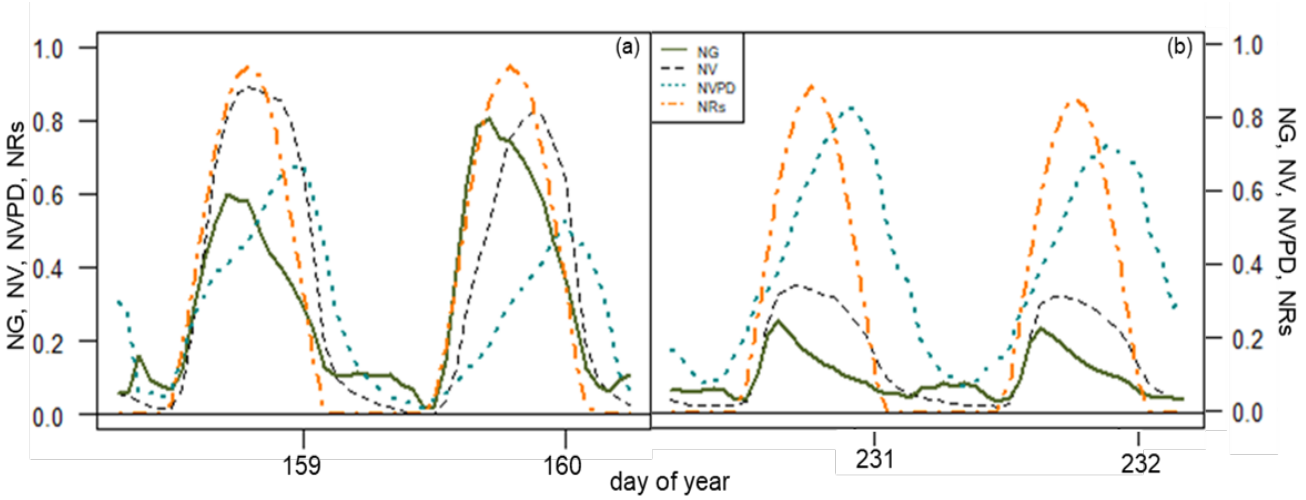

Figure 10. Diurnal traces of normalized vapor pressure deficit (NVPD), solar radiation (NRs), sap velocity (NV) and isothermal canopy conductance (NG) in an illustrative tree during two contrasting water status periods (a) early and (b) late season in 2016.

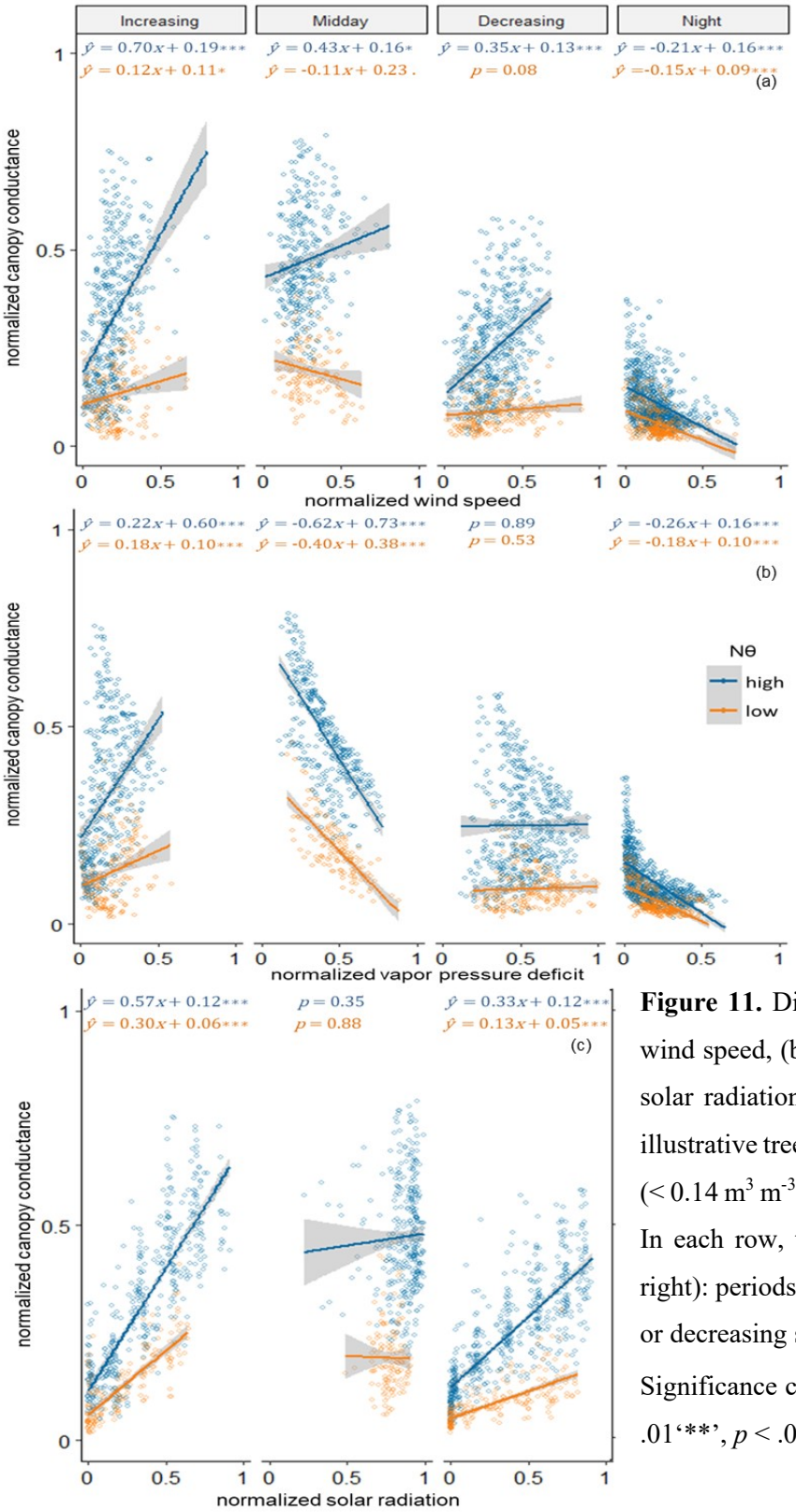

Figure 11. Diurnal effects of normalized (a) wind speed, (b) vapor pressure deficit and (c) solar radiation on canopy conductance in an illustrative tree at high (> 0.14 m^3 m^{-3}) and low (< 0.14 m^3 m^{-3}) soil water contents (θ) in 2016. In each row, the panels denote (from left to right): periods of increasing, mid-day (steady) or decreasing solar radiation, and night-time. Significance codes: $p > .05$‘.’, $p < .05$‘*’, $p < .01$‘**’, $p < .001$‘***’

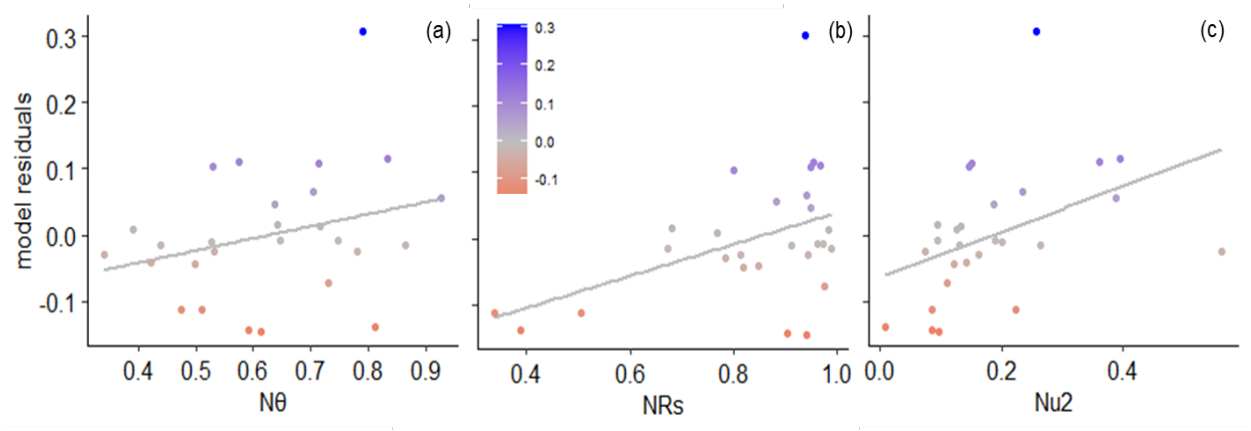

Figure 12. The relationship of model residuals of normalized canopy conductance (NG) and midday stem water potential (Ψ_{stem}) between normalized (a) soil water content (Nθ), (b) solar radiation (NRs) and (c) wind speed (Nμ2) from averaged measurements obtained on all eight trees during both 2016 and 2017 seasons. Symbol colors denote values of the residuals.

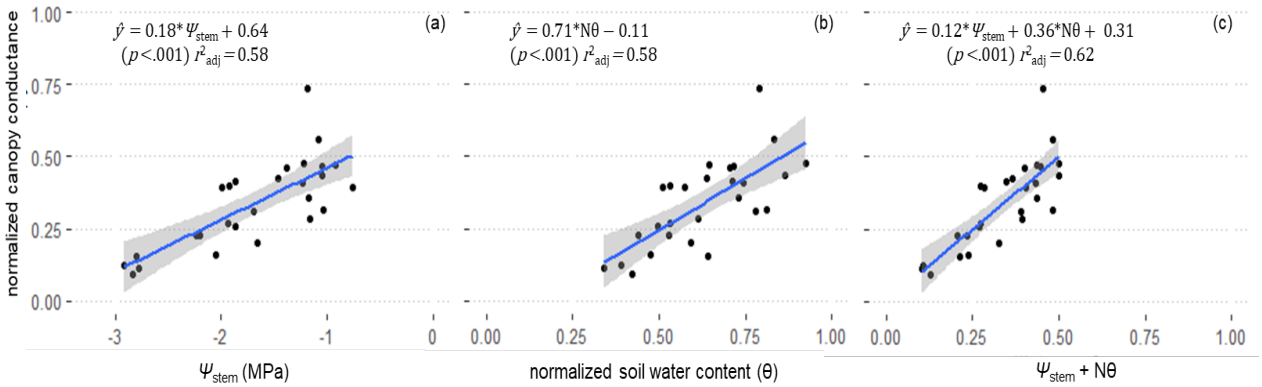

Figure 13. Normalized canopy conductance as predicted by (a) midday stem water potential (Ψ_{stem}), (b) normalized soil water content (Nθ) and (c) both Ψ_{stem} + Nθ. Data were averaged for all trees on days and times that midday Ψ_{stem} was measured.